Ramsey-Bordé Matter-Wave Interferometry for Laser Frequency Stabilization at 10^{-16} Frequency Instability and Below

Judith Olson,[1,2,*] Richard W. Fox,[1] Tara M. Fortier,[1] Todd F. Sheerin,[3,4] Roger C. Brown,[1] Holly Leopardi,[1,2]
Richard E. Stoner,[4] Chris W. Oates,[1] and Andrew D. Ludlow[1,2,†]

[1]*Time and Frequency Division, National Institute of Standards and Technology, Boulder, Colorado 80305, USA*
[2]*Department of Physics, University of Colorado, Boulder, Colorado 80309, USA*
[3]*Department of Aeronautics and Astronautics, Massachusetts Institute of Technology, Cambridge, Massachusetts 02139, USA*
[4]*The Charles Stark Draper Laboratory, Inc., Cambridge, Massachusetts 02139, USA*

We demonstrate Ramsey-Bordé (RB) atom interferometry for high performance laser stabilization with fractional frequency instability $< 2 \times 10^{-16}$ for timescales between 10 and 1000s. The RB spectroscopy laser interrogates two counterpropagating ^{40}Ca beams on the $^1S_0 - {}^3P_1$ transition at 657 nm, yielding 1.6 kHz linewidth interference fringes. Fluorescence detection of the excited state population is performed on the $(4s4p)\ ^3P_1 - (4p^2)\ ^3P_0$ transition at 431 nm. Minimal thermal shielding and no vibration isolation are used. These stability results surpass performance from other thermal atomic or molecular systems by 1 to 2 orders of magnitude, and further improvements look feasible.

Lasers with exceptional frequency stability play a foundational role in fundamental physics, precision measurement, and technological applications. Noteworthy is the optical clock, which derives its unmatched measurement precision from a frequency-stabilized laser locked to a narrowband atomic resonance [1,2]. Such precision enables searches for both dark matter and variations of fundamental constants [3–5] while motivating redefinition of the International System second [6]. Ultrastable lasers are key components in many tests of relativity [7–9] and lie at the heart of gravitational wave observatories [10–12]. They are used in quantum control and manipulation, including recent explorations of SU(n) interactions and quantum simulation [13,14]. Furthermore, their stability can be readily transferred [15,16] across the electromagnetic spectrum for advanced communication and radar systems or next-generation position, navigation, and timing.

We present a method for ultraprecise laser-frequency stabilization based on Ramsey-Bordé (RB) matter-wave interferometry using a thermal calcium beam. This approach enables frequency instability $< 2 \times 10^{-16}$ and possesses a vibration sensitivity that could be orders of magnitude smaller than the standard workhorse of optical frequency stabilization, the Fabry-Perot cavity. Such cavities typically employ high quality factor (Q) and signal to noise (S/N), offering impressive 10^{-16} instability at short times, with recent progress on very long [17] and cryogenic [18,19] cavities reaching into the 10^{-17} decade. This performance level is important for minimizing the Dick effect in optical clocks and enabling coherent interrogation of ultralong-lifetime atomic states [20]. Yet increasing challenges of further reducing cavity thermal noise [21] have spurred research in alternative approaches aimed at circumventing the thermal noise problem, including super-radiant lasers [22–24] and spectral hole burning [25].

Here, we employ optical Ramsey techniques [26,27] common to atom interferometry and precision measurements [28–32]. Our specific design builds upon the experimental geometry laid out in [33]. This technique was chosen for its ability to resolve narrow spectral features from a high-flux thermal beam of atoms or molecules despite their large velocity distribution. In this way, the traditionally problematic trade-offs in atomic systems between Q and S/N can be avoided, enabling both relatively fast and precise frequency corrections. To our knowledge, this is the first time a thermal frequency reference has demonstrated stability at $\leq 10^{-15}$, highlighting an entirely new regime of performance. This unlocks new applications for thermal ensembles, which are simpler than cold-atom systems and generally possess superior long-term stability and accuracy over mechanical references such as cavities.

Ramsey-Bordé interferometry [33] employs four $\pi/2$ laser-atom interactions that repeatedly split the atomic wave function, resulting in two closed quantum trajectories (Fig. 1) that encode interferometric fringes on the atomic state populations [28]. The excited state probability, P_e, is a periodic function of the interrogation laser frequency, ν, around the natural transition frequency, ν_0, given by the energy difference between atomic states, as well as the phase difference, $\Phi = \phi_2 - \phi_1 + \phi_4 - \phi_3$, accumulated from each sequential laser interaction of phase ϕ_i (Fig. 1) such that
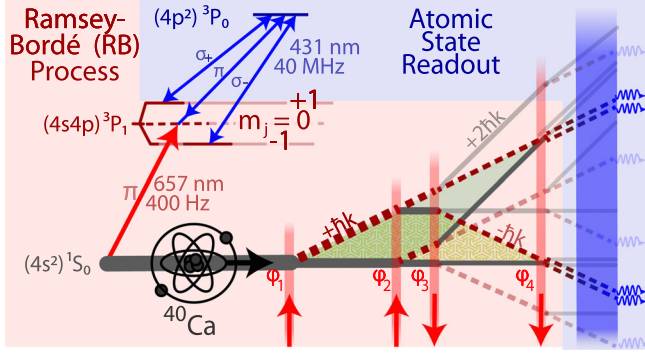
FIG. 1. Relevant electronic levels and transitions of neutral ^{40}Ca. Also shown is the quantum trajectory of a calcium atom passing through the RB interferometer. The atom undergoes four laser interactions with phase ϕ_i, which repeatedly split the atomic momentum state. Two possible closed trajectories exist (filled areas), creating matter-wave interference. The $^3P_1 - ^3P_0$ transition is then rapidly cycled, and the scattered 431 nm photons collected.

$$P_e \propto \cos[4\pi(\nu - \nu_0 \pm \delta\nu_{\mathrm{recoil}} + \nu_{\mathrm{sys}})T + \Phi], \quad (1)$$

where T is the free-evolution time (i.e., Ramsey time) between the first and second, or equivalently, the third and fourth laser interactions. The atomic recoil frequency is $\delta\nu_{\mathrm{recoil}} = h/2m\lambda^2 \cong 11.5$ kHz for the $^1S_0 - ^3P_1$ transition in calcium, where h is Planck's constant, λ is the transition wavelength, and m is the atomic mass. All other systematic frequency shifts, such as those caused by stray fields or time dilation, are included in ν_{sys}. While the RB technique is ideally free from first-order Doppler shifts, residual
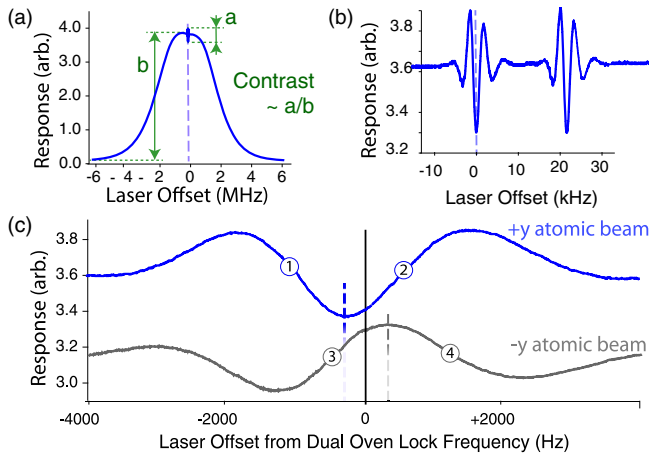

FIG. 2. Typical RB fringes for a range of frequency sweeps. (a) MHz scale Doppler profile of one atomic beam response, with accompanying measure of fringe contrast. (b) Midrange sweep displaying two RB fringe components from a single atomic beam. (c) Simultaneous fine sweep across the RB fringes from both counterpropagating atomic beams. Dashed lines indicate extrema feature frequencies, and points 1 to 4 indicate four locking frequency locations.

first-order Doppler effects are traditionally included in the fringe phase, Φ. T varies across the ensemble's broad Maxwell-Boltzmann velocity distribution [34], yielding only a few resolvable RB fringe periods, as seen in Fig. 2.

Two thermal beams of calcium atoms are used for frequency correction. These counterpropagating beams are defined by the same apertures to precisely overlap (Fig. 3). Atoms from opposing ovens experience the interferometer in reverse orders, causing the total accumulated phase, Φ, of each oven's fringe to be nominally equal and opposite. Therefore, locking the laser frequency to the bidirectional average reduces sensitivity to residual first-order Doppler shifts from optical path length variation, imperfect interferometer alignment, and RB laser input angle. Though a technique reversing laser propagation on a single atomic beam was also employed [35], we observed fringes with more robust antisymmetry from dual atomic beams, ultimately yielding better laser stability.

The fundamental vibrational insensitivity of the RB interferometer can be appreciated through comparison to a Fabry-Perot cavity. Thermomechanical noise and acceleration-induced cavity deformation often limit the stability of the Fabry-Perot cavity, causing an optical path length change, δl, corresponding to a fractional frequency shift $\delta\nu/\nu = \delta l/l_{\mathrm{cav}}$, for cavity length l_{cav}. For the RB interferometer, a similar change in optical path yields a phase difference, $\Delta\Phi = 2\pi(\delta l/\lambda)$. From Eq. (1), the resulting fractional frequency shift is $\delta\nu/\nu = [(\delta l/\lambda)(1/2T)]/\nu = (\delta l/l_{\mathrm{RB}})(v_{\mathrm{atom}}/2c)$, where v_{atom} (l_{RB}) is the atomic velocity (distance traveled) during T. For the reasonable approximation $l_{\mathrm{cav}} \approx l_{\mathrm{RB}}$ (here, $l_{\mathrm{RB}} = 9$ cm), optical-path-length driven frequency shifts to the RB system are reduced by a factor $v_{\mathrm{atom}}/2c \sim 10^{-6}$ compared to the Fabry-Perot cavity. On the other hand, because atoms in a RB interferometer are free bodies, accelerations alter their trajectory relative to the laser field, introducing a frequency shift sensitivity predominantly along the laser propagation axis [36], $\delta\nu/\nu = l_{\mathrm{RB}}a/v_{\mathrm{atom}}c$ for acceleration a. For parameters listed above, this corresponds to a fractional-frequency acceleration sensitivity of $\delta\nu/\nu = 5 \times 10^{-12}a/g$, for gravitational acceleration g. While this acceleration sensitivity is already competitive with the best Fabry-Perot cavity designs [37,38], the atomic beam reversal technique employed here allows further sensitivity reduction.

A natural choice of quantum absorber for RB-interferometer-based laser stabilization is calcium, using the $^1S_0 - ^3P_1$ clock transition at 657 nm (Fig. 1) with an excited state lifetime near 400 μs [36,39,40]. Because the RB fringe linewidth decreases as $1/T$, an ideal RB interferometer interrogates the atoms for a time approaching the natural lifetime. For calcium effusing from an oven near 625 °C with average speed > 600 m/s, this requires an interferometer length of $\sim$20 cm, well suited to a compact apparatus.
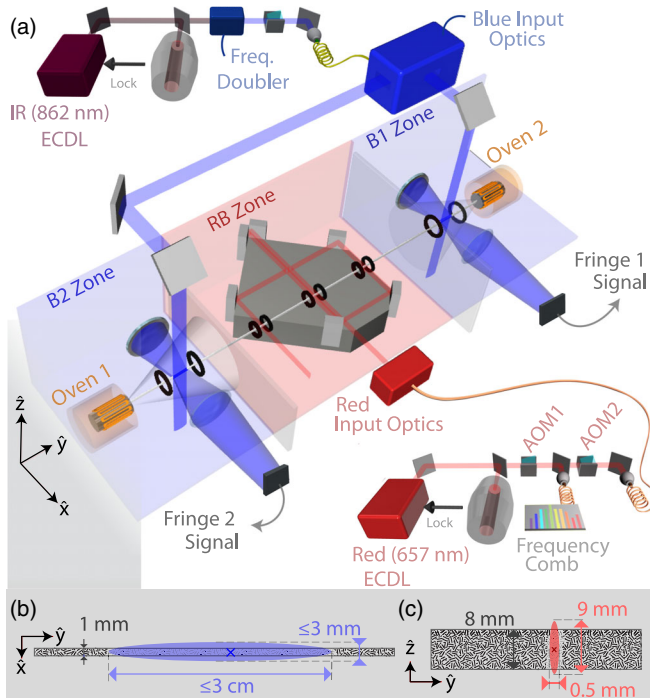
FIG. 3. Experimental setup. (a) Both 862 nm (later frequency doubled to 431 nm) and 657 nm lasers are cavity prestabilized. Input optics mounted on the vacuum chamber shape and deliver the light. The vacuum chamber is partitioned into two blue detection zones ($B1$ and $B2$) and the RB zone. Within vacuum, the interrogation laser is steered by a monolithic glass assembly to intersect the atomic beam at four locations. The distance between beams 1 and 2 (or 3 and 4) is 9 cm, whereas the spacing between beams 2 and 3 is roughly 1 mm. In regions $B1$ and $B2$, exited-state atoms are rapidly cycled while their scatter is focused onto an external detector. Magnetic fields are indicated by black coils. Apertures between zones collimate the atomic beams. AOM: acousto-optic modulator; ECDL: external cavity diode laser. [(b) and (c)] Approximate blue (431 nm) and red (657 nm) laser profiles, respectively, are given relative to the atomic beam dimensions. Typical laser powers are 10 (431 nm) and 25 mW (657 nm), incident on the atoms.

Additionally, ^{40}Ca possesses a relatively strong transition from the RB excited state to a doubly excited state, $(4s4p)$ $^3P_1 - (4p^2)$ $^3P_0$ at 431 nm (Fig. 1). A second laser resonantly applied to this transition is used for electron-shelving fluorescence detection [41] of the RB fringes, enabling hundreds of photons to be emitted per atom without appreciable optical pumping into dark states. Both the 657 and 431 nm sources are accessible with commercially available diode lasers, with sufficient power to efficiently drive these transitions.

The calcium apparatus uses a vacuum chamber with pressure near 10^{-5} Pa, which is partitioned symmetrically into three zones (Fig. 3). The intensity- and phase-stabilized 657 nm interrogation laser is delivered to the RB zone through a viewport and then directed along a nearly meter-long folded path in vacuum with exacting parallelism. This is accomplished via an ultralow-expansion (ULE) glass spacer with angular tolerances ~1 arcsecond. The spacer sits below beam line with optically contacted high-reflection ULE mirrors extending beyond the plane of the interrogation laser. Also in the central RB zone, the magnetically insensitive $^3P_1$ ($m_J = 0$) sublevel is spectrally isolated from $m_J = \pm 1$ with ≈ 700 μT fields during RB interrogation.

Elsewhere, laser light at 431 nm is intensity stabilized, shaped, and split into two paths for delivery to the blue detection zones ($B1$ and $B2$ in Fig. 3). Each of these zones employs a single Helmholtz coil pair to generate an ~800 μT field over the approximately 3 cm long laser-atom interaction [Fig. 3(b)]. Of the hundreds of photons scattered by each excited-state atom, approximately 10% are imaged onto a detector (Fig. 3). The blue laser polarization incident on the atomic beam is adjusted to optimize the collected laser-induced fluorescence.

Both laser beam profiles at 657 and 431 nm, as well the atomic beam profile, are steeply elongated in one dimension. The atomic beam is shaped by fine apertures before and after the RB zone, restricting its profile to 1×8 mm. The laser profiles are shaped using anamorphic prism pairs. All relevant beam dimensions are given in Figs. 3(b) and 3(c). The red beam's narrow waist increases transit time broadening at each RB interaction zone to address a larger range of velocity classes without appreciable impact on the fringe linewidth. However, the short Rayleigh range prevents uniform collimation throughout the in-vacuum optical path. Taken together with wavefront imperfections and inhomogeneous pulse area from the thermal beam velocity distribution, fringe contrast is reduced. In theory, contrast can reach 25%, though optimized values between 13% and 18% were observed. Interestingly, contrast is typically maximized when the interrogation laser is either slightly convergent or divergent.

Frequency corrections are generated by monitoring the fluorescence amplitude at four distinct interrogation laser frequencies—two for each fringe feature [Fig. 2(c)]. The frequencies are modulated with an acousto-optic-modulator (AOM2 in Fig. 3). For each oven the corresponding fluorescence levels are sampled and compared, and the two-oven average generates the frequency corrections via AOM1 (Fig. 3). The frequency difference between the two fringe extrema is tracked to accommodate relative phase variations between atomic beams. A single experimental cycle, including fluorescence collection, AOM updates, and 4 ms of dead time, is 10–30 ms.

The RB-stabilized laser instability is assessed via a frequency comb referenced to a ytterbium optical lattice clock system with instability $< 10^{-16}$ after averaging ≈ 10 s [42]. On shorter times, the Yb clock instability is largely derived from an advanced Fabry-Perot cavity with
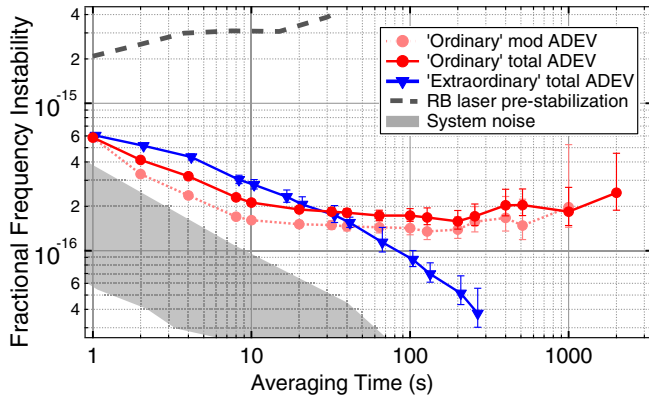
FIG. 4. Allan deviations for two calcium-stabilized frequency measurements with 1σ error bars. The general system performance is well represented by the data set labeled ordinary (red circles), whereas extraordinary (blue triangles) highlights shorter data segments exhibiting exceptional performance, averaging below 10^{-16}. The RB laser prestabilization is shown after a 2 Hz/s drift removal, though this drift is present during calcium system operation. The measured range of frequency instability contributions from detection noise sources falls within the gray region; see the text.

instability $\leq 2 \times 10^{-16}$ at 1 s. Utilizing these two stable references and the low noise frequency comb ensures meaningful measurements of the ^{40}Ca stabilized laser frequency for all timescales presented here.

We evaluate the frequency stability of the system for data sets taken over two timescales: one ordinary set over 1.4 hours and one extraordinary set over 10 minutes. Both are plotted in Fig. 4, where the red curves represent typical (ordinary) performance, which employs basic temperature control of the apparatus at the $\sim$10 mK level. Instability near 2×10^{-16} could be maintained for timescales of an hour, during which a flicker noise floor dominates around 1.2×10^{-16}. These data include a $\sim$100 μHz/s measured drift. As laser stability is sometimes reported with the modified ADEV stability estimator, this is also displayed in Fig. 4.

The extraordinary blue curve of Fig. 4 averages into the 10^{-17} decade over $\sim$10 minutes of frequency measurements. Similar instability can be seen for periods up to 20 minutes, usually after the apparatus has run continuously for some time. This data set employed no temperature stabilization, and a linear frequency drift near 1 mHz/s was removed for the analysis. Averaging over longer intervals yields instability closer to that of the ordinary data in Fig. 4. In general, RB stabilization with this system yields 1 s performance between 3 and 8×10^{-16} with linear frequency drifts of ≤ 1 mHz/s. Importantly, all stability levels presented were observed both with and without vibration isolation.

The gray region in Fig. 4 denotes a range of detection noise, measured by tuning the 657 nm laser away from the RB fringes but still on the Doppler pedestal [Fig. 2(a)] and

then scaling the fluctuations in detected fluorescence by the fringe discriminator slope, which yields the corresponding frequency fluctuations. This noise is a combination of photon shot noise and technical detector noise, and our measured frequency instability falls near this noise level for periods < 10 s. At longer time intervals, we observed that temperature fluctuations of the apparatus typically correlate strongly with frequency wander. We also investigated other sources of instability that were found to be less significant, including fluctuations in magnetic fields, laser intensity and polarization, laser pointing, vacuum levels, vibrations, atomic beam flux, and atomic collisions [43].

The exceptional instability demonstrated here compared to other thermal systems is facilitated by four important design considerations. First, the high atomic flux (10^{10} to 10^{12} atoms per second) yields an atom shot-noise limited frequency instability $\leq 10^{-17}$ at short times, rivaling future thermal noise limits in cryogenically cooled optical cavities. Second, dual ovens allow cancellation of fringe-phase (Φ) drifts that otherwise degrade mid- and long-term performance. Third, enclosing the RB laser path within vacuum suppresses deleterious phase and pointing noise. Lastly, the excited-state cycling detection scheme used here is quite efficient—even after accounting for solid angle collection and detector quantum efficiency, most atoms contribute $\gg 1$ photon to the resulting frequency correction.

A number of efforts look promising towards improving either the short-term stability (via improved detection system, atomic beam parameters, and fringe contrast) or the long-term performance (via temperature stabilization). For example, segmented RB interrogation using distinct pairs of phase-stabilized lasers could enhance fringe contrast closer to the fundamental limit of 25%, whereas simultaneous interrogation of both RB recoil components could yield a straightforward $\sqrt{2}$ enhancement in S/N. Measurements of the RB system temperature sensitivity suggest that 1 mK stability could support stability at the 10^{-17} level. This could make the calcium RB system compelling as an optical flywheel in a next-generation optical time scale, akin to the role played by hydrogen masers in conventional time scales.

However, the performance demonstrated here is already intriguing in the search for physics beyond the standard model. Benefiting from relatively high bandwidth and S/N, the calcium RB system enables searches for dark-matter interactions at mass and timescales beyond the reach of most optical clocks [44,45]. Furthermore, the simplicity and precision of our system could be exploited for isotope shift measurements in the search for new interactions via King's plot nonlinearities [46]. Though the full potential of the RB system has not yet been seen, the instability results demonstrated here, combined with the system's low vibration sensitivity, atom-number scalability, and compact size, make RB

---

*judith.olson@colorado.edu
†andrew.ludlow@nist.gov

[1] N. Nemitz, T. Ohkubo, M. Takamoto, I. Ushijima, M. Das, N. Ohmae, and H. Katori, Nat. Photonics **10**, 258 (2016).

[2] N. Huntemann, C. Sanner, B. Lipphardt, C. Tamm, and E. Peik, Phys. Rev. Lett. **116**, 063001 (2016).

[3] Y. Stadnik and V. V. Flambaum, Phys. Rev. A **93**, 063630 (2016).

[4] A. Derevianko and M. Pospelov, Nat. Phys. **10**, 933 (2014).

[5] M. S. Safronova, D. Budker, D. DeMille, D. F. Jackson Kimball, A. Derevianko, and C. W. Clark, Rev. Mod. Phys. **90**, 025008 (2018).

[6] F. Riehle, C.R. Phys. **16**, 506 (2015).

[7] N. Ashby, T. E. Parker, and B. R. Patla, Nat. Phys. **14**, 822 (2018).

[8] I. Georgescu, Nat. Phys. **13**, 529 (2017).

[9] C.-W. Chou, D. Hume, T. Rosenband, and D. Wineland, Science **329**, 1630 (2010).

[10] B. P. Abbott, R. Abbott, T. D. Abbott, M. R. Abernathy, F. Acernese, K. Ackley, C. Adams, T. Adams, P. Addesso, R. X. Adhikari et al. (LIGO Scientific and Virgo Collaborations), Phys. Rev. Lett. **116**, 061102 (2016).

[11] F. Acernese, M. Agathos, K. Agatsuma, D. Aisa, N. Allemandou, A. Allocca, J. Amarni, P. Astone, G. Balestri, G. Ballardin et al., Classical Quantum Gravity **32**, 024001 (2015).

[12] B. Canuel, A. Bertoldi, L. Amand, E. Pozzo di Borgo, T. Chantrait, C. Danquigny, M. Dovale lvarez, B. Fang, A. Freise, R. Geiger et al., Sci. Rep. **8**, 14064 (2018),

[13] X. Zhang, M. Bishof, S. L. Bromley, C. V. Kraus, M. S. Safronova, P. Zoller, A. M. Rey, and J. Ye, Science **345**, 1467 (2014).

[14] F. Schmidt-Kaler, H. Häffner, M. Riebe, S. Gulde, G. P. Lancaster, T. Deuschle, C. Becher, C. F. Roos, J. Eschner, and R. Blatt, Nature (London) **422**, 408 (2003).

[15] H. Leopardi, J. Davila-Rodriguez, F. Quinlan, J. Olson, J. A. Sherman, S. A. Diddams, and T. M. Fortier, Optica **4**, 879 (2017).

[16] X. Xie, R. Bouchand, D. Nicolodi, M. Giunta, M. Hnsel, M. Lezius, A. Joshi, S. Datta, C. Alexandre, M. Lours et al., Nat. Photonics **11**, 44 (2017).

[17] S. Häfner, S. Falke, C. Grebing, S. Vogt, T. Legero, M. Merimaa, C. Lisdat, and U. Sterr, Opt. Lett. **40**, 2112 (2015).

[18] D. G. Matei, T. Legero, S. Häfner, C. Grebing, R. Weyrich, W. Zhang, L. Sonderhouse, J. M. Robinson, J. Ye et al., Phys. Rev. Lett. **118**, 263202 (2017).

[19] J. M. Robinson, E. Oelker, W. R. Milner, W. Zhang, T. Legero, D. G. Matei, F. Riehle, U. Sterr, and J. Ye, Optica **6**, 240 (2019).

[20] Y. Jiang, A. Ludlow, N. D. Lemke, R. W. Fox, J. A. Sherman, L.-S. Ma, and C. W. Oates, Nat. Photonics **5**, 158 (2011).

[21] K. Numata, A. Kemery, and J. Camp, Phys. Rev. Lett. **93**, 250602 (2004).

[22] M. A. Norcia, J. R. K. Cline, J. A. Muniz, J. M. Robinson, R. B. Hutson, A. Goban, G. E. Marti, J. Ye, and J. K. Thompson, Phys. Rev. X **8**, 021036 (2018).

[23] S. A. Schäffer, B. T. R. Christensen, S. M. Rathmann, M. H. Appel, M. R. Henriksen, and J. W. Thomsen, J. Phys. Conf. Ser. **810**, 012002 (2017).

[24] Y.-F. Wang and J.-B. Chen, Chin. Phys. Lett. **29**, 073202 (2012).

[25] S. Cook, T. Rosenband, and D. R. Leibrandt, Phys. Rev. Lett. **114**, 253902 (2015).

[26] J. Bergquist, S. Lee, and J. Hall, Phys. Rev. Lett. **38**, 159 (1977).

[27] R. Barger, J. Bergquist, T. English, and D. Glaze, Appl. Phys. Lett. **34**, 850 (1979).

[28] C. J. Bordé, Phys. Lett. A **140**, 10 (1989).

[29] T. Kovachy, P. Asenbaum, C. Overstreet, C. Donnelly, S. Dickerson, A. Sugarbaker, J. Hogan, and M. Kasevich, Nature (London) **528**, 530 (2015).

[30] P. Hamilton, M. Jaffe, P. Haslinger, Q. Simmons, H. Müller, and J. Khoury, Science **349**, 849 (2015).

[31] B. Dubetsky, S. B. Libby, and P. Berman, Atoms **4**, 14 (2016).

[32] J. Keupp, A. Douillet, T. E. Mehlstäubler, N. Rehbein, E. M. Rasel, and W. Ertmer, Eur. Phys. J. D **36**, 289 (2005).

[33] C. J. Bordé, C. Salomon, S. Avrillier, A. Van Lerberghe, C. Bréant, D. Bassi, and G. Scoles, Phys. Rev. A **30**, 1836 (1984).

[34] R. Barger, Opt. Lett. **6**, 145 (1981).

[35] N. Ito, J. Ishikawa, and A. Morinaga, Opt. Commun. **109**, 414 (1994).

[36] G. Wilpers, C. Degenhardt, T. Binnewies, A. Chernyshov, F. Riehle, J. Helmcke, and U. Sterr, Appl. Phys. B **76**, 149 (2003).

[37] S. Webster and P. Gill, Opt. Lett. **36**, 3572 (2011).

[38] D. R. Leibrandt, J. C. Bergquist, and T. Rosenband, Phys. Rev. A **87**, 023829 (2013).

[39] J. J. McFerran and A. N. Luiten, J. Opt. Soc. Am. B **27**, 277 (2010).

[40] H. Shang, X. Zhang, S. Zhang, D. Pan, H. Chen, and J. Chen, Opt. Express **25**, 30459 (2017).

[41] W. Nagourney, J. Sandberg, and H. Dehmelt, Phys. Rev. Lett. **56**, 2797 (1986).

[42] W. McGrew, X. Zhang, R. Fasano, S. Schäffer, K. Beloy, D. Nicolodi, R. Brown, N. Hinkley, G. Milani, M. Schioppo et al., Nature (London) **564**, 87 (2018).

[43] J. Olson, Ph.D. thesis, University of Colorado, 2019.

[44] P. Wcisło, P. Morzyński, M. Bober, A. Cygan, D. Lisak, R. Ciuryło, and M. Zawada, Nat. Astron. **1,** 0009 (2017).

[45] Y. V. Stadnik and V. V. Flambaum, Phys. Rev. Lett. **114,** 161301 (2015).

[46] J. C. Berengut, D. Budker, C. Delaunay, V. V. Flambaum, C. Frugiuele, E. Fuchs, C. Grojean, R. Harnik, R. Ozeri, G. Perez, and Y. Soreq, Phys. Rev. Lett. **120,** 091801 (2018).